Article ID: 1006-8775(2020) 02-0150-11

A Precipitation Detection Method for MWTS−II Radiance Assimilation in Typhoon Simulation

YUAN Bing (袁 炳), MA Gang (马 刚), ZHANG Peng (张 鹏),
XI Shuang (希 爽), WANG Ting-fang (王廷芳)
(Satellite Meteorological Research Division, National Satellite Meteorological Center, Beijing 100083 China)

Abstract: FY-3C Microwave Temperature Sounder II (MWTS-II) lacks observations at 23.8 GHz, 31 GHz and 89 GHz, making it difficult to remove the data contaminated by precipitation in assimilation. In this paper, a fast forward operator based on the Community Radiative Transfer Model (CRTM) was used to analyze the relationship between the observation minus background simulation (O-B) and the cloud fractions in different MWTS-II channels. In addition, based on the community Gridpoint Statistical Interpolation (GSI) system, the radiation brightness temperature of the MWTS-II was assimilated in the regional Numerical Weather Prediction (NWP) model. In the process of assimilation, Visible and Infrared Radiometer (VIRR) cloud detection products were matched to MWTS-II pixels for precipitation detection. For typhoon No. 18 in 2014, impact tests of MWTS-II data assimilation was carried out. The results show that, though the bias observation minus analysis (O-A) of assimilated data can be reduced by quality control only with | O-B | < 3K; however, the O-A becomes much smaller while the precipitation detection is performed with $F_{virr} < 0.9$ (VIRR cloud fraction threshold of 0.9). Besides, the change of the environmental field around the typhoon is more conducive to make the simulated track closer to the observation. The 72-hour typhoon track simulation error also shows that, after the precipitation detection, the error of simulated typhoon track is significantly reduced, which reflects the validity of a precipitation detection method based on a double criterion of | O-B | < 3K and $F_{virr} < 0.9$.

Key words: numerical weather prediction; MWTS-II data assimilation; precipitation cloud detection; track simulation of typhoon
CLC number: P4 **Document code:** A
https://doi.org/10.46267/j.1006-8775.2020.014

1 INTRODUCTION

Assimilation of satellite observations has been one of the most significant methods to improve the accuracy of Numerical Weather Prediction (NWP) in recent 30 years. Satellite data have been successively assimilated into operational global NWP models both in the European Center of Medium Weather Forecast (ECMWF) and the National Center for Environmental Prediction (NCEP) [1,2,3,4]. Results from the operation showed that more than 30 satellite observations had been used, which accounts for over 95% of all data assimilation observations[5]. Advanced Microwave Sounder Unit-A (AMSU-A) data is currently one of the most influential satellite observations for model predictions, which can provide profiles of atmospheric temperature from the ground to 3 hPa with 12 channels set by O_2 absorption line at 50GHz. Assimilation of these AMSU-A radiance made significant impact on model forecasts[6, 7].

In the assimilation method, temperature and humidity are transformed from the model to the channel radiation observed by satellite using linear fast radiation transfer operator [8, 9]. Then the three-dimensional distribution of atmospheric temperature and humidity in the initial field of the model is optimized by narrowing the difference between simulated radiation and AMSU-A observations. The forward modeling of AMSU-A data in clear sky only considers the absorption and emission of O_2, and the observation minus background simulation (O-B) is less than 1K[10]. However, a large O-B value might be found in cloudy atmosphere due to the strong scattering of hydrometers with multi-phases to microwave radiation[11], despite regressed look-up tables both in the Radiative Transfer model to TOVs (RTTOV) and the Community Radiative Transfer Model (CRTM) were used to account for scattering of cloud liquid water, rain water, cloud ice, snow and graupel. At present, all-sky assimilation has been achieved in global NWP operation of the ECMWF and the NCEP. However, in many other operations and researches, only clear sky radiance of AMSU-A is used [12,13,14,15]. Therefore, together with the bias correction [16,17], precipitation detection of microwave data become an important skill to ensure a high quality of clear sky AMSU-A satellite

Received 2019-10-12; **Revised** 2020-02-15; **Received** 2020-05-15
Foundation items: Natural Science Foundation of China (41505082); Special Scientific Research Fund of Meteorology in the Public Welfare Profession of China (GYHY201506002, GYHY201506022)
Biography: YUAN Bing, Ph. D., primarily undertaking the research on numerical simulation and data assimilation.
Corresponding author: MA Gang, e-mail: magang@cma.gov.cn

data be integrated into assimilation system.

Generally, the precipitation detection of 50 GHz microwave observation mainly uses the observation of 23 GHz and 31 GHz channels to simulate the brightness temperature of 89GHz channels, and uses the threshold of O-B to judge whether the pixel is contaminated by precipitation or not [18,19,20]. Although FY-3C MWTS-II has 13 channels at 50GHz, compared with AMSU-A, there are no observations channels at 23Hz, 31GHz and 89GHz for such a traditional precipitation detection method. Although precipitation contamination could be partially eliminated by using high quality O-B information from the ECMWF [21,22], an effective precipitation detection scheme is still necessary for assimilating Clear Sky Data. On the other hand, precipitation must occur in the cloudy atmosphere, and there must be a correlation among cloud fraction, cloud water and precipitation. The Visible and Infrared Radiometer (VIRR) of FY-3c is used to observe surface and cloud with a 1.1km resolution at nadir of visible and near-infrared spectrums. The cloud mask at resolution of VIRR could be mapped onto pixels of FY-3C InfraRed Atmosphere Sounder (IRAS) at arbitrary zenith angle by a fusion method in the area of sensor's pixel projected on ground [23,24]. Experiments at the National Meteorological Center (NMC) of Chinese Meteorological Administration (CMA) showed that precipitation can be identified in MWTS-II pixels when mapped cloud fraction is beyond 0.6 from the VIRR cloud mask, and obtained a positive impact on global model forecast by assimilating MWTS-II radiance while using it as precipitation detection [25]. Indeed, the water particles of non-precipitation clouds also can absorb and emit microwave radiation, but it is worth further discussing whether the threshold of 0.6 may cause the loss of observation information by excessively removing useful data. In other words, the sensitivity of assimilation analysis to cloud amount should be further discussed, so as to determine a more reasonable threshold.

In this paper, the CRTM fast radiation transfer mode was used, and the sensitivity of MWTS-II channel simulated radiance to mapped VIRR cloud cover was analyzed. Compared with FY2 cloud cover data, a cloud amount was determined as the threshold of precipitation detection. With an assimilation operator of MWTS-II brightness temperature used in the regional three-dimensional variational assimilation system, and with a typhoon case, the assimilation experiment of MWTS-II data was carried out to estimate the performance of a new precipitation detection scheme with an appropriate cloud amount threshold.

2 DATA AND THEORY

2.1 *FY-3C MWTS-II*

FY-3C was successfully launched on September 23, 2013 and was the first operational satellite of the second generation polar orbit meteorological satellite of China. MWTS-II, with 13 channels of O_2 absorption line at 50GHz, is one of the most important atmosphere temperature sounders with higher vertical resolution in the satellite. As a cross-track step scanning sensor with a scan period of 8 / 3 s, a field angle of 2.2º and a maximum field angle of ± 49.5°, it features 90 foot-points per scan line, and the nadir resolution of the foot-points is original 45 km, and 15 km with a sampling technique.

The weight function of the channel reflects the detection height, and is defined as:

$$w_f = \partial\tau/\partial \ln P \quad (1)$$

where w_f is the weighting function of a channel, τ is the layer transmittance of the channel, and P is the pressure. Weighting function of MWTS-II channels was calculated by using US1976 standard profile and is shown in Fig.1. The atmospheric temperature profile can be detected from surface to 3hPa by MWTS-II. The peak height of weights in channel 1 and channel 2 are near the ground, and thus the channel radiance cannot be used into assimilation due to the inaccuracy of surface emissivity. Since the top of the regional model layer is 10 hPa (horizontal straight line), the peak height of weight in channels 10 is too close to the model top, and the peak height of weights in channels 11, 12 and 13 are higher than the model top. Therefore, the radiance data of channel 3-9 was selected for assimilation.

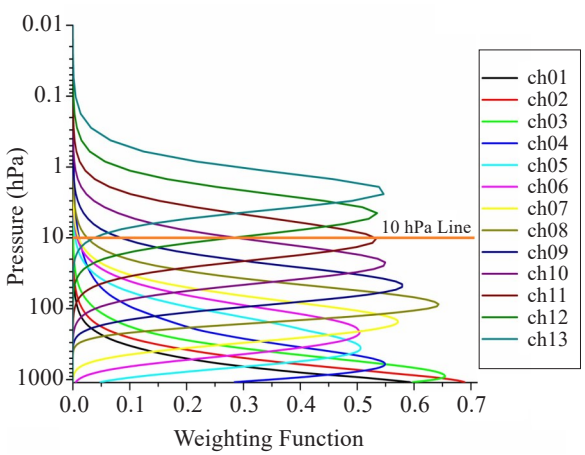

Figure 1. Weighting function of MWTS-II channels.

2.2 *FY-3C VIRR and its cloud mask*

VIRR on FY-3 is a visible/near infrared radiometer with 10 channels. As a cross-track step scanning sensor with a scan period of 1/6s, and a maximum scan angle of ± 55.4°, VIRR features 2048 foot-points per scan line, and the resolution of the foot-points is 1.1 km at nadir. Infrared and near infrared channels of VIRR are at window spectrum and seldom sensitive to absorbers, such as CO_2, water vapor and ozone. Therefore, visible and near infrared channels of VIRR are used to retrieve cloud mask at daytime, and near infrared and infrared channels are designed to obtain cloud mask at nighttime.

Thresholds of multi-features defined as deviation or ratio of observations among channels are used to identify the cloud mask of VIRR, both in a single channel and a channel group. Then dynamic thresholds by histogram and thresholds lookup-table by simulation are used to yield the cloud mask thresholds. Finally, a complex analysis is carried out based on cloud mask from single cloud detection to identify whether it is clear or cloudy to a VIRR pixel [23].

2.3 *Mapping data from VIRR pixel to MWTS-II pixel*

Mapping is to calculate the representative observation values from an instrument field of view (FOV) to another instrument FOV which has a new resolution, and to identify the view angles from mapped instrument to target instrument. In order to ensure the consistent resolution of various observations, a lookup table is established to evaluate weights of every mapped observation from the target view angle.

For the observations and the geographical parameters of all foot-points, a mapping model is set up at grid-points to connect satellite observations data between mapping sensor and target sensor. Considering both the orbital stepping direction and the scanning direction, the shift to a target foot-point on stepping direction is determined by a temporal gap between the starting time of the scan line and the time of the target foot-point, and the shift to the foot-point on scanning direction is calculated by serial number of the target foot-point and geometrical parameters of the sensor observation mode. In a rectangle, when N_{cld} is the number of cloudy foot-point that has been mapped into the target pixel, N_{clr} is the number of clear mapped pixels, D_N is cloud fraction of target foot-point, then it can be represented as:

$$D_N = \frac{N_{\mathrm{cld}}}{N_{\mathrm{cld}} + N_{\mathrm{clr}}} \tag{2}$$

therefore, the cloud fraction that is between 0 and 1 can be found in MWTS-II pixel when cloud masks at 1.1 km resolution are mapped onto pixels with a resolution of 15km.

VIRR cloud masks are superposed into a visible image of FY-2 near observation time in Fig. 2a. It is indicated that the VIRR cloud masks correctly identify the cloud distribution in the weather system, and these cloud masks coincide completely with the cloud revealed in FY-2 image over ocean. Mapped cloud fraction in MWTS-II pixels are revealed in Fig. 2b and the color bar are cloud fraction values. Regions with cloud fraction larger than 0.9 are covered by the cloud of typhoon system (see Fig. 2a) and the typhoon shape is unclear for the resolution decreasing from 1.1km to 15km. However, the mapped cloud fraction is between 0.1 and 0.6 in peripheral cloud of the typhoon. Then, we can draw a conclusion that the cloud distribution of typhoon system can be indicated correctly by mapped cloud fraction in MWTS-II pixels with values between 0 and 1 in degraded resolution.

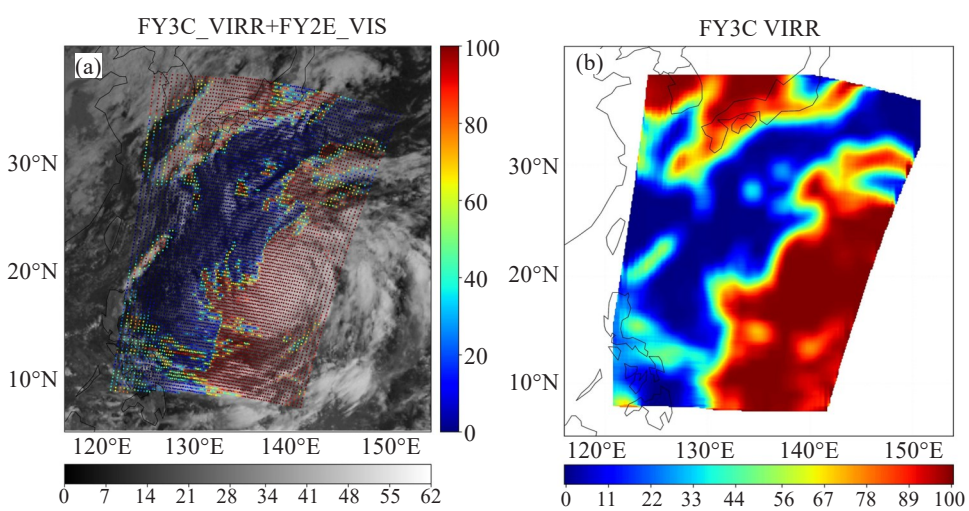

Figure 2. VIRR cloud masks vs. FY2 image (a) and cloud masks mapped to MWTS-II pixel (b). The multi-color bar in (a) is cloud fraction (0-100 means fraction of 0-1) on VIRR pixel, the black-white bar in (a) is albedo scaling index of FY2 image, and the color bar in (b) is the value scale of mapped cloud fraction (similarly 0-100 means fraction of 0-1) on MWTS-II pixel.

3 RELATIONSHIP BETWEEN CLOUD FRACTION AND O-B IN MWTS-II PIXELS

3.1 *Sensitive analysis of mapped cloud fraction to observations*

To identify the sensitivity of mapped cloud fraction to observed radiation in various MWTS-II channels, an algorithm is developed to calculate the microwave radiation from semi-cloud cover in MWTS-II pixel in the CRTM.

$$L_i = (1 - N)\cdot L_i^{\mathrm{clr}} + N\cdot L_i^{\mathrm{cld}} \tag{3}$$

L is the radiation at each channel. N is cloud fraction in a foot-point. Subscript i is the serial number of channels, and superscript clr and cld indicate clear case and cloudy

case respectively. The deviations of simulation at clear case and at various cloud fractions are revealed in channels in assimilation of Fig. 3. The channel 5 observation is insensitive to cloud fraction, except when the cloud fraction is 0.9 (with a deviation of 0.015K). Detection heights from channel 6 to channel 9 are higher than that of channel 5, and the O-B of these channels no longer vary along with cloud fraction. For other channels with a height of peak weighting function lower than channel 5, the maximum deviation of channel 3 is 0.3K with a cloud fraction of 0.9, and tiny deviations could be found when the cloud fraction is smaller than 0.9. Thus the conclusion can be drawn that large deviations only exist in lower channels due to cloud or precipitation emission and scattering, and 0.9 can be the threshold to identify contamination by precipitation because large deviations can be observed when the cloud fraction is larger than the threshold in lower channels.

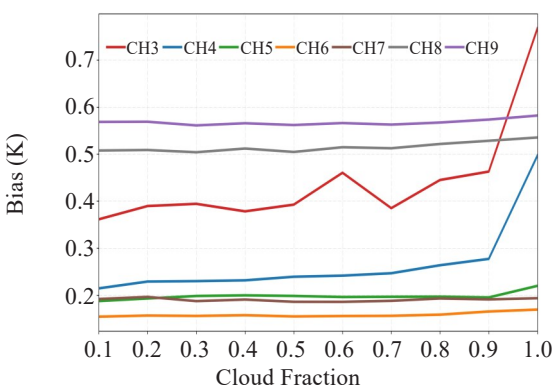

Figure 3. O-B to MWTS-II data of channels used in assimilation with various cloud fractions thresholds.

When various mapped cloud fractions (F_{virr} is 0.2, 0.4, 0.6, 0.8, 0.9 and 1.0 respectively) are used as the precipitation detection thresholds, the MWTS-II channel 3 observations kept after the "precipitation detection" are shown in Fig.4. The visible image of FY-2 is used as the base map. The typhoon center located in the east of the FY-3C orbit region and most MWTS-II observations are over ocean. Almost all observations can be introduced into assimilation except for a little data over land when the threshold of cloud fraction is 1.0. Due to stricter "precipitation detection", the smaller observations of MWTS-II were kept while a smaller mapped cloud fraction was used as the threshold. Observations in the east and south of the typhoon are rejected, and the data in the west of the typhoon is kept except for that near 135ºE, 22ºN when the threshold is 0.9. However, little number variation of the observations can be found in assimilations with variance of mapped cloud fraction. When the mapped cloud fraction threshold is 0.2, the sky in the west and north of typhoon is "clear". And near 138ºE, 25ºN, the MWTS-II observations, with small mapped cloud fractions threshold, only can be injected over the thin cirrus cloud band area of the typhoon.

3.2 *Impact on O-B*

Taking the observations of MWTS-II channel 3 as an example, Fig. 5 shows the number of assimilated observations, as well as the variations of O-B and O-A. Different mapped cloud fractions (0.2, 0.4, 0.6, 0.8, 0.9 and 1.0) are set in 6 profiles in Fig. 5. *X*-axis is the number of observations used in assimilation. More observations can be assimilated while the mapped cloud fraction increases from 0.2 to 1.0. There are less than

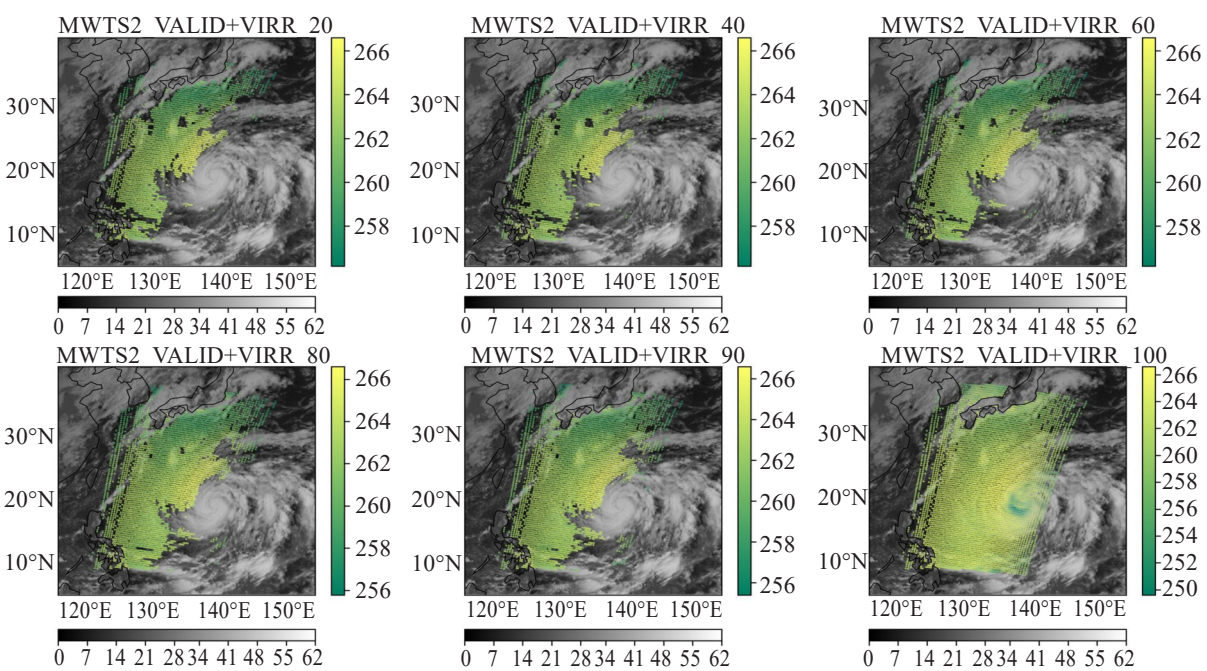

Figure 4. Observations (units: K) of channel 3 kept after precipitation detection with various cloud fraction thresholds (the black-white bar is albedo scaling index of FY2 image, and the multi- color bar is MWTS-II channel 3 brightness temperature (units: K); VIRR_xx represents cloud fractions (0-100 means fractions of 0-1).

4,000 observations assimilated when the mapped cloud fraction is 0.2. Observations used in assimilation slowly increase to 6,000 when the mapped cloud fraction grows from 0.2 to 0.9. Observations are over 10,000 in assimilation when the mapped cloud fraction turns into 1.0. *Y*-axis is the value of O-B and O-A. In Fig. 5, red line indicates O-B of every observation, and green line indicates O-A of the same observations. The systematic bias of O-B is −3K, and changes within an range of [−1K, −8K]. When the mapped cloud fraction grows from 0.2 to 1.0, the systematic bias of O-B is within −4K, and the variation interval of O-B changes from [−1K, −8K] to [−1K, −4.5K]. It is noted that most O-B are concentrated in the variation interval of [−1K, −5K] when the mapped cloud fraction is 0.9. After assimilation, systematic bias of O-A is removed, and a variation interval of [−2K, 2K] can be found when the mapped cloud fraction is 0.9. And it is obvious that the O-A is mostly −3K in samples' interval of [500, 2500] only when the mapped cloud fraction is 1.0. Therefore, the O-A can be reduced when the mapped cloud fraction is used as a quality control factor during the MWTS-II data assimilation. The number of injected MWTS-II observations shows enormous differences when the mapped cloud fraction is 0.9, and the same situation can be found in O-B and O-A. In other words, when the cloud fraction of the map is less than 0.9, the difference between the observed values O-B and O-A is smaller.

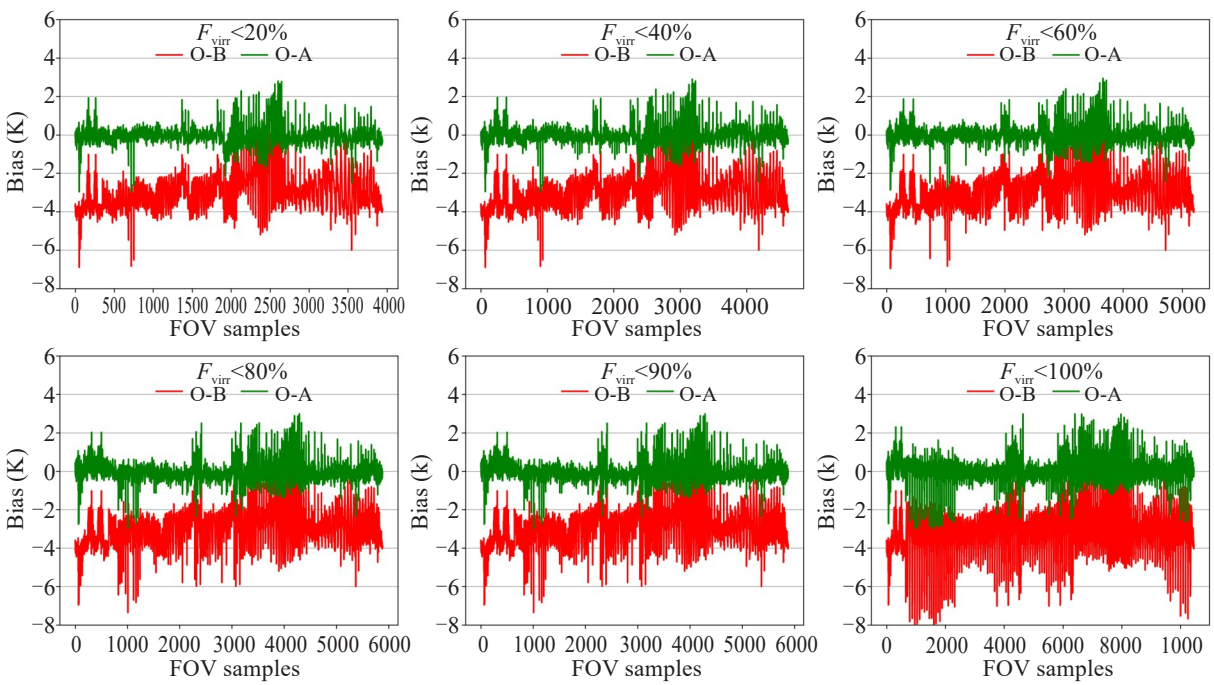

Figure 5. O-B and O-A of MWTS-II channel 3 data with various cloud fraction as thresholds for precipitation detection.

The PDF (Probability Density Function) variations in both O-B and O-A of MWTS-II channel 3 in various mapped cloud fractions are shown in Fig. 6, with the same mapped cloud fractions as in Fig. 5. Primary deviations are in the interval of [−2K, −4K] in any mapped cloud fraction before assimilation. When the mapped cloud fraction threshold increases from 0.2 to 1.0, the probability of O-B decreases at −4K and increases at −2K, but gradually reduces in [−2K, 0K]. Few variations can be found in PDF shape while the mapped cloud fraction is less than 0.9. However, the PDF grows quickly in [−4K, −6K] when the mapped cloud fraction is 1.0. PDF of channel 3 data is unbiased Gaussian distribution at 0K after the assimilation. When the mapped cloud fraction increases from 0.2 to 0.9, and locating the PDF to 3×10^{-4}, the O-A can be found mainly in [−1.3K, 1.3K]. And when the mapped cloud fraction is 1.0, with the same PDF, the O-A is in [−1.5K, 1.5K]. It is shown that, the smaller mapped cloud fraction used as the threshold of precipitation detection, the criterion for removing those observations contaminated by precipitation would be stricter. The impact of precipitation is weak on O-B when the mapped cloud fraction is less than 0.9. And good unbiased Gaussian distribution of PDF in O-A can be found in these microwave observations after a quality control by the mapped cloud fraction.

Figure 7a shows the distribution of channel 3 observations that pass a quality check with only | O-B |< 3K. It did not use the mapped cloud fraction to perform precipitation detection. Fig. 7b shows the distribution of O-B and O-A. Compared with the observations in Fig. 4, most of observations were retained both in clear and cloudy pixels, even if the strong convection covered the typhoon area. This leads to the lack of calculation of the scattering, absorption and emission of precipitable particles in the calculation of radiation transfer under the assumption of clear sky, resulting in inaccurate

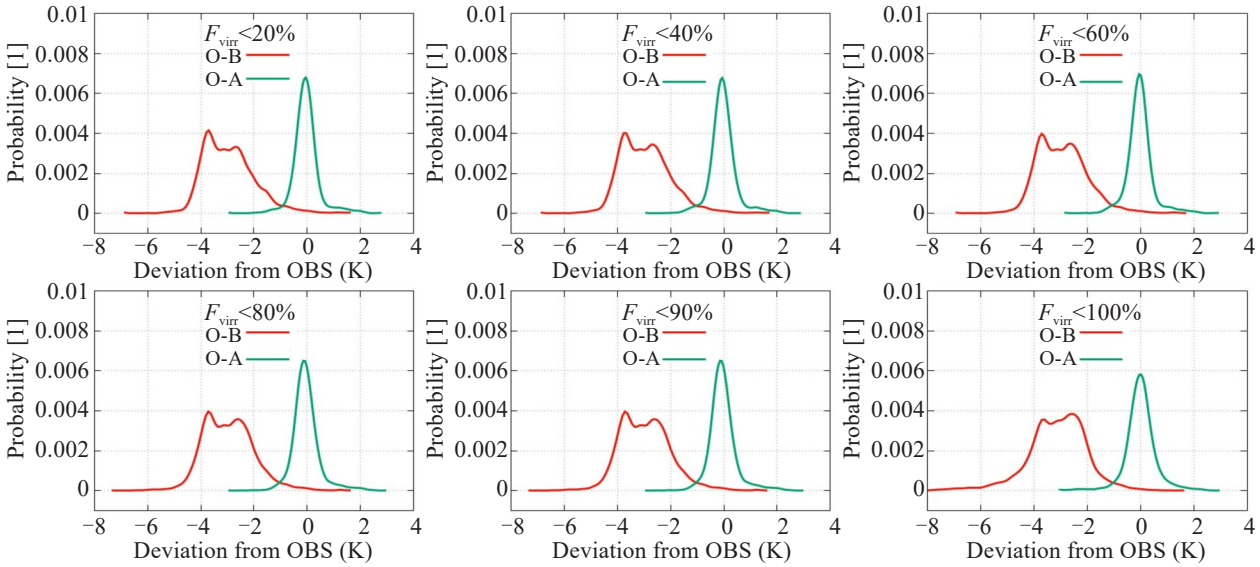

Figure 6. PDF of O-B and O-A of MWTS-II channel 3 data with various mapped cloud fraction as thresholds for precipitation detection.

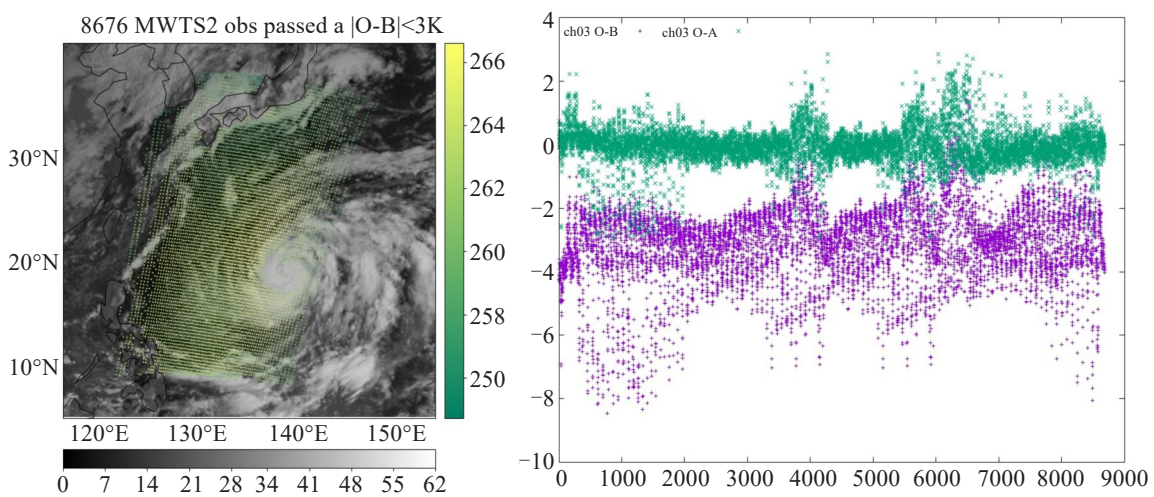

(a) Observations used in assimilation (b) O-B and O-A of channel 3 of MWTS-II data

Figure 7. Impact on the number of observations, O-B and O-A when only the threshold of |O-B|<3K is used for quality control. In (a), the black-white bar is albedo scaling index of FY2 image, and the multi-color bar is MWTS-II channel 3 brightness temperature (units: K). In (b), the *x*-axis is FOV samples of observations, and the *y*-axis is bias.

adjustment of the distribution of atmospheric temperature and humidity in the initial field of NWP model. In Fig. 7, more than 9000 observations were retained, and the systemic bias of O-B is −3K before the assimilation. After the assimilation, the systemic bias is removed. However, the O-A is in the interval of [−1, 3K], which is larger than the range of O-A in quality control by the mapped cloud fraction. Therefore, though both the observations with large O-B and the systemic bias of O-B can be removed when only the threshold of O-B is used as a quality control, it is unreasonable that those MWTS-II data, introduced into assimilation after the quality control, is in strong convective region of typhoon. And various ranges of O-A were greater than that after a quality control by mapped cloud fraction.

4 EXPERIMENTS AND RESULTS

4.1 *Introduction of the typhoon case*

The 18th typhoon occurred at 2pm, September 29, 2014 and had a track far from the main land. It quickly weakened into an extratropical cyclone near Tokyo on the afternoon of October 6. An assimilation cycle with 4 assimilations per 12 hours is used to identify the impact of the precipitation detection method on analysis and forecast of MWTS-II data assimilation since 00UTC, October 2, 2014.

4.2 *Assimilation system and forecast model*

As a 3D variation assimilation system, GSI was developed by the NCEP and was used to analyze the assimilations of various observations into numerical

forecast model. Direct assimilation of satellite radiance data has been carried out in GSI due to the integration of forward and adjoint model of CRTM. A fast radiative transfer model of FY-3C MWTS-II, based on the frame of CRTM, was developed in the National Satellite Meteorological Center (NSMC) and was introduced into GSI to assimilate MWTS-II radiance data. A variety of quality controls were integrated into the assimilation and the cloud fraction mapped from VIRR was used as the threshold for precipitation detection.

Advanced physical parameterization and nest domain had been included in the Weather Research and Forecasting (WRF) model. As a non-hydrostatically balanced and fully compressible dynamic model, the Arakawa C grid is used in the WRF in the horizontal direction, and the terrain is followed by Sigma coordinates in the vertical direction. Coarse domain grids are 45km, and 51 levels are set in vertical direction while the top level of the model is 10hPa. For single nest in the WRF, fine domain grids are at 15km horizontal resolution with the same set of vertical levels and model top as in the coarse domain.

4.3 *Test schemes*

GSI-based assimilation has a 6-hour assimilation window, and 72-h forecasts of the typhoon was simulated by the WRF. Analysis fields of T639--a global NWP model in CMA is used as initial fields. The experiment started at 00UTC, October 2, 2014, and performed 4 assimilations of MWTS-II radiance data per 12 hours cycle. Every 6h prediction of the typhoon from WRF is used to test the impact of the assimilation. During the experiment, three schemes are shown in Table 1. Two quality controls are built for the assimilation. No precipitation detection in method A, which means observations contaminated by precipitation are simplely rejected by a threshold of O-B. In method B, mapped cloud fraction of VIRR (F_{virr}) was set at 0.9 as a threshold to conduct precipitation detection. Then a comparison was carried out to test the analysis and forecast. Besides, a surface interpolation method of minimum sea-level pressure is used to located the center of typhoon[26].

Table 1. Numerical experiment schemes.

No.	The Initial Scheme	
Scheme 1	Control experiment with initial field from T639	(CTRL)
Scheme 2	MWTS-II radiance assimilation with |O-B|<3K	(QC method A)
Scheme 3	MWTS-II radiance assimilation with |O-B|<3K and F_{virr} <0.9	(QC method B)

4.4 *Results and analyses*

The typhoon location could be distinguished by the MWTS-II data image of channel 1 that with a peak height of weighting function near surface. MWTS-II Observations of channel 1 are displayed in all the 4 assimilation windows in Fig. 8. The interval between neighbor assimilation windows is 12 hours because of a regular 12 hour period of the polar-orbit every day. In addition, 6-h assimilation window can ensure that one or two orbits of FY-3C are included in the test region. For example, there was one orbit in assimilation window at 00UTC and two orbits at 12UTC. The typhoon center was at 140ºE, 19ºN, the edge of an orbit of FY-3C, and only a dim non-spiral clouds could be found around 135ºE, 20ºN at 00UTC, October 2. Typhoon's clouds could be distinguished at 134ºE, 20ºN when the typhoon was in the middle of an FY-3C orbit at 12UTC, October 2. It was the same in satellite image at 00UTC, October 3. and the typhoon eye could be distinguished at 12UTC, Otc. 3, though a part of the typhoon was in a gap between two orbits. Therefore, tremendous efficient satellite observations can be introduced into data assimilation for that most typhoon clouds were covered by MWTS-II observations. Both the typhoons' structure and track can be improved by assimilating the satellite data in and out of the region of the typhoon.

Figure 9 shows the background potential height, potential height increments of scheme A and scheme B after assimilation, and the difference between the two increments, on 850hPa, 500hPa and 200HPa, at 00UTC, Oct. 2. In the figure, columns 1, 2 and 3 respectively are 850 hPa, 500 hPa and 200 hPa. On 850 hPa, the typhoon shows a strong low-value area. There are high-pressure areas in the northeast and west of the typhoon, and a low-pressure area in the northwest (125ºE, 40ºN). The assimilation in scheme A weakens the typhoon, but increases the geopotential heights in the northeast and south of the typhoon, and decreases the geopotential heights in the west of the typhoon, which is conducive to the westward movement for the typhoon. In scheme B, because of observations contaminated by precipitation in the typhoon areas was removed by precipitation detection, the weakening of typhoon is alleviated, and the potential height over land increases, which may prevent the westward movement of typhoon conversely. In addition, an obvious positive potential height increment in the southwest of typhoon is beneficial to the northward movement of the typhoon. A similar situation occurred at 500 and 200 hPa. By comparing the two schemes, it can be seen that, the deviation between the two quality control methods in the geopotential height field adjustment is mainly the difference of the increment range, which may make the typhoon's future movement trend be different.

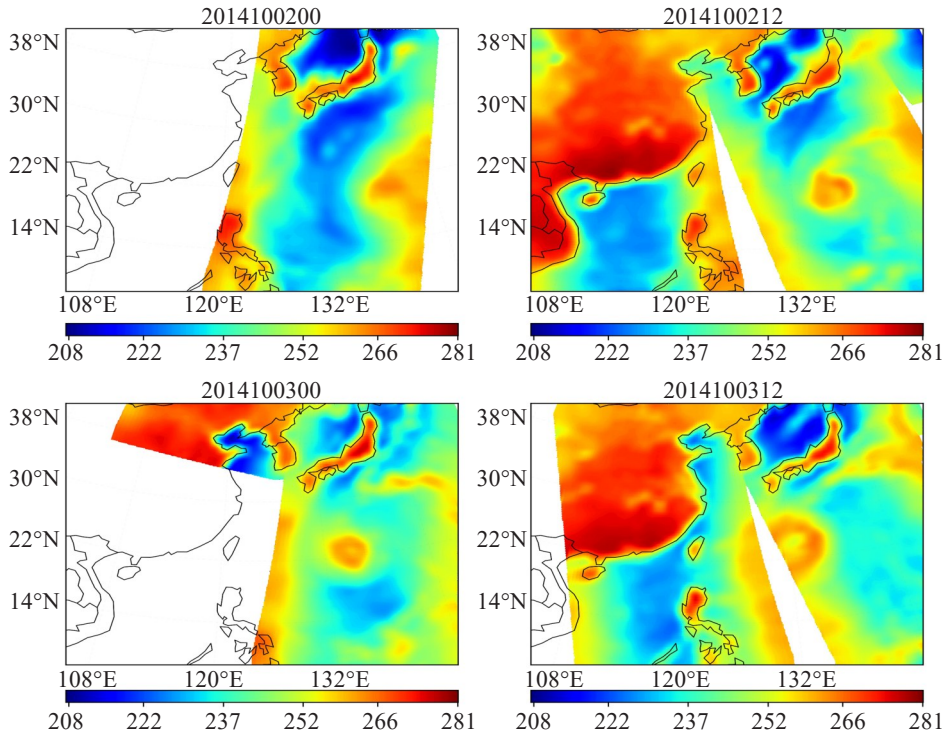

Figure 8. Observations of MWTS-II channel 1 in 4 assimilations' windows.

In each experiment, after assimilating MWTS-II data, the 72-h simulations of the typhoon were performed. The simulated tracks of 4 times and the biases are revealed in Fig. 10. In the experiment with a quality control method that |O-B| <3K (method A, marked as 'Qc_OMB'), good performances can only be obtained in cycle 2014100212 and cycle 2014100312. But when a mapped cloud fraction threshold of 0.9 (F_{virr} <0.9) is added (method B, marked as 'Qc_OMB+CLD'), good performances can be obtained in all cycles, and an obvious improvement in track simulation can be found in 'Qc_OMB' experiments (except for an interval of [24hours, 60hours] in cycle 2014100212), compared with control experiments. For all track simulations, the track deviation means the distance error of tracks between simulation and observation. The track deviations in 'Qc_OMB + CLD' tests, compared with control experiments or 'Qc_OMB' experiments, has largely decreased. For example, in the forecast interval [48hours, 72hours] of cycle 2014100212, compared with control experiment, the deviation decreases almost 500km. And particularly, in cycles 2014100200 and 2014100300, compared with 'Qc_OMB' experiments, track deviations respectively decrease 800km and 500km at 72 hours forecast.

5 CONCLUSIONS

In this paper, a fast forward operator based on the CRTM was used to calculate the MWTS-II microwave radiation, and the sensitivity of radiation brightness temperature calculation to the mapped cloud fraction from VIRR was analyzed for MWTS-II channels. The assimilation system for MWTS-II radiation brightness temperature based on GSI model was used, and the cloud fraction mapped from VIRR was used for precipitation detection. And assimilation and forecast experiments of typhoon No. 18 in 2014 were carried out for impact evaluation. Compared with the traditional quality control method using O-B threshold, the efficiency of a new quality control method with the mapped cloud fraction for precipitation detection was verified. The main conclusions are listed as follows.

(1) The forward calculation and analysis of MWTS-II radiation brightness temperature shows that the cloud fraction has little effect on the high-level channel. For low and middle level channels, only when the cloud fraction is greater than 0.9 will a greater impact occur. Thus, the cloud fraction of 0.9 can be used as the criterion to judge whether MWTS-II observation is contaminated by precipitation.

(2) As a quality control of MWTS-II data, precipitation detection by mapped cloud fraction from VIRR can reduce the deviation of assimilated observation data. When the cloud fraction threshold is set to 0.9, the number of assimilated MWTS-II observations varies prominently, and the O-B and O-A change greatly before and after assimilation. However, the assimilation of MWTS-II observations, O-B and O-A change smoothly when the threshold is less than 0.9.

(3) Using O-B threshold for quality control can eliminate large and systematic deviation of observation data after assimilation. However, MWTS-II data can still be distributed in severe precipitation area, which is contrary to the original intention of precipitation

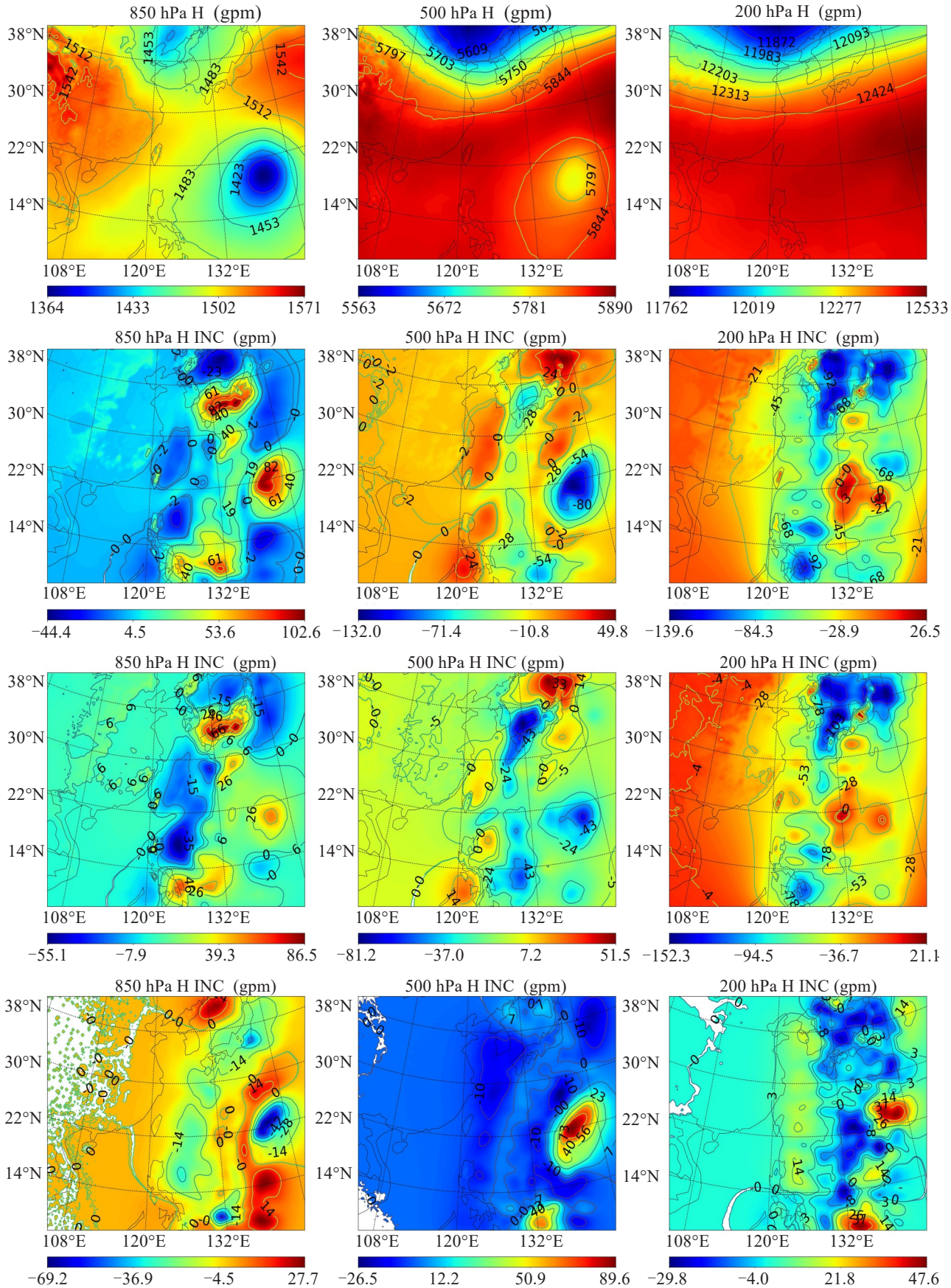

Figure 9. The geopotential height in control experiment (1st row), the geopotential height increment in method A(2nd row), the geopotential height increment in method B(3rd row), and the difference between the increments in two methods(4th row, B minus A) on 850hPa(1st column), 500hPa(2nd column) and 200hPa(3rd column) respectively, at 00UTC, October 2.

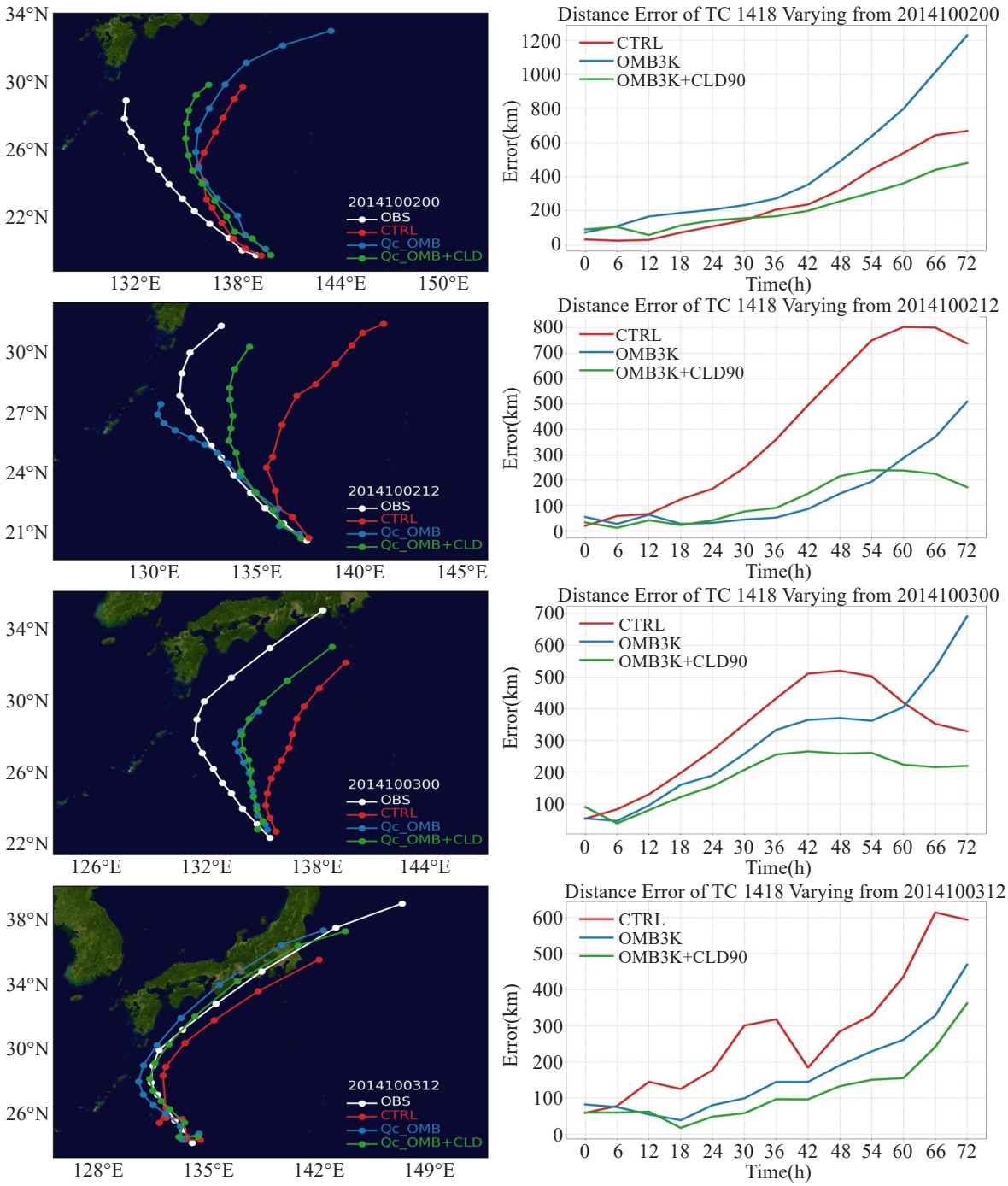

Figure 10. Impact on typhoon's 72-h simulated tracks (left) and deviations (right) by assimilation of MWTS-II radiance in 4 cycles.

detection. And the O-A is significantly larger than that considering mapped cloud fraction for precipitation detection.

(4) Thresholds of O-B and mapped cloud fraction were used as quality control schemes for MWTS-II radiation data assimilation respectively. By comparing the two schemes, it can be seen that, the deviation between the two quality control methods in geopotential height field adjustment is mainly the difference of the increment range, which may make the typhoon's future movement trend different.

(5) 72-h simulations of typhoon were made in 4 cycles. Deviations between simulated and observed tracks revealed that in the test with quality control of a 3K threshold of |O-B|, a good performance can only be obtained in a few cycles when compared to the control test. After a threshold of 0.9 of the mapped cloud fraction from VIRR was added as a additional quality control, it performs well in all cycles, and an obvious reduction of deviations is achieved both in comparisons with control experiments and with experiments using a 3K threshold of |O-B| as quality control only. It demonstrates the effectiveness of the precipitation detection method with |O-B| <3K and F_{virr}<0.9 as a

double criterion.

REFERENCES

[1] DERBER J C, WU W S. The use of TOVS cloud-cleared radiances in the NCEP SSI analysis system [J]. Mon Wea Rev, 1998, 126(8): 2287-2299, https://doi. org / 10.1175 / 1520-0493(1998)126<2287:TUOTCC>2.0.CO;2.

[2] BOUTTIER F, KELLY G. Observing - system experiments in the ECMWF 4D - Var data assimilation system [J]. Quart J Roy Meteorol Soc, 2001, 127(574): 1469-1488, https:// doi.org/10.1002/qj.49712757419.

[3] KLINKER E, RABIER F, KELLY G, et al. The ECMWF operational implementation of four-dimensional variational assimilation, III: Experimental results and diagnostics with operational configuration [J]. Quart J Roy Meteorol Soc, 2000, 126(564): 1191-1215, https://doi. org / 10.1002 / qj.49712656417.

[4] ANDERSSON E, PAILLEUX J, THEPAUTT J N, et al. Use of cloud-cleared radiances in three / four-dimensional variational data assimilation [J]. Quart J Roy Meteorol Soc, 1994, 120(517): 627-653, https://doi. org / 10.1002 / qj.49712051707.

[5] RABIER F. Overview of global data assimilation developments in numerical weather - prediction centres [J]. Quart J Roy Meteorol Soc, 2005, 131(613): 3215-3233, https://doi.org/10.1256/qj.05.129.

[6] ENGLISH S J, RENSHAW R J, DIBBEN P C, et al. A comparison of the impact of TOVS arid ATOVS satellite sounding data on the accuracy of numerical weather forecasts [J]. Quart J Roy Meteorol Soc, 2010, 126(569): 2911-2931, https://doi.org/10.1002/qj.49712656915.

[7] MCNALLY A P, DERBER J C, WU W, et al. The use of TOVS level-1b radiances in the NCEP SSI analysis system [J]. Quart J Roy Meteorol Soc, 2000, 126(563): 689-724, https://doi.org/10.1002/qj.49712656315.

[8] SAUNDERS R, MATRICARDI M, BRUNEL P. An improved fast radiative transfer model for assimilation of satellite radiance observations [J]. Quart J Roy Meteorol Soc, 2015, 125(556): 1407-1425, https://doi. org / 10.1002 / qj.1999.49712555615.

[9] WENG F. Advances in radiative transfer modeling in support of satellite data assimilation [J]. J Atmos Sci, 2007, 64(64): 3799-3807, https://doi. org / 10.1175 / 2007JAS2112.1.

[10] MATRICARDI M, CHEVALLIER F, KELLY G, et al. An improved general fast radiative transfer model for the assimilation of radiance observations [J]. Quart J Roy Meteorol Soc, 2004, 130(596): 153-173, https://doi. org / 10.1256/qj.02.181.

[11] BAUER P, MOREAU E, CHEVALLIER F, et al. Multiple-scattering microwave radiative transfer for data assimilation applications [J]. Quart J Roy Meteorol Soc, 2006, 132(617): 1259-1281, https://doi. org / 10.1256 / qj.05.153.

[12] POWERS J G, GAO K. Assimilation of DMSP and TOVS satellite soundings in a mesoscale model [J]. J Appl Meteorol, 2000, 39(10): 1727-1741, https://doi. org / 10.1175/1520-0450-39.10.1727.

[13] BAUER P, GEER A J, LOPEZ P, et al. Direct 4D - Var assimilation of all - sky radiances, Part I: Implementation [J]. Quart J Roy Meteorol Soc, 2010, 136(652): 1868-1885, https://doi.org/10.1002/qj.659.

[14] GEER A J, BAUER P, LOPEZ P. Direct 4D - Var assimilation of all - sky radiances, Part II: Assessment [J]. Quart J Roy Meteorol Soc, 2010, 136(652): 1886-1905, https://doi.org/10.1002/qj.681.

[15] ZHU Y, LIU E, MAHAJAN R, et al. All-sky microwave radiance assimilation in the NCEP's GSI analysis system [J]. Mon Wea Rev, 2016, 144(12): 4709-4735, https://doi. org/10.1175/MWR-D-15-0445.1.

[16] HARRIS B A, KELLY G. A satellite radiance - bias correction scheme for data assimilation [J]. Quart J Roy Meteorol Soc, 2001, 127(574): 1453-1468, https://doi.org/ 10.1002/qj.49712757418.

[17] YANG Y, HAN W, DONG P M. Overview on the quality control in assimilation of AMSU microwave sounding data [J]. Meteorol Mon, 2011, 37(11): 1395-1401, https:// doi.org/10.1007/s00376-010-1000-5.

[18] WENG F, ZHAO L, FERRARO R R, et al. Advanced microwave sounding unit cloud and precipitation algorithms [J]. Radio Science, 2003, 38(4): 8068, https:// doi.org/10.1029/2002rs002679.

[19] FERRARO R R, WENG F, GRODY N C, et al. NOAA operational hydrological products derived from the advanced microwave sounding unit [J]. IEEE Transactions on Geoscience& Remote Sensing, 2005, 43 (5): 1036-1049, https://doi.org/10.1109/tgrs.2004.843249.

[20] BENNARTZ R, THOSS A, DYBBROE A, et al. Precipitation analysis using the advanced microwave sounding unit in support of nowcasting applications [J]. Meteorol Appl, 2002, 9(2): 177-189, https://doi. org / 10.1017/s1350482702002037.

[21] LU Q, BELL W, BAUER P, et al. Characterizing the FY-3A microwave temperature sounder using the ECMWF model [J]. J Atmos & Oceanic Technol, 2011, 28(11): 1373-1389, https://doi.org/10.1175/JTECH-D-10-05008.1.

[22] WANG Y H, LEE G, HE G X. A quality control procedure for FY-3 microwave radiance data [J]. Transactions of Atmos Sci, 2013, 36(5): 560-567 (in Chinese).

[23] WANG X, LI W, ZHU Y, et al. Improved cloud mask algorithm for FY-3A / VIRR data over the northwest region of China [J]. Atmospheric Measurement Techniques, 2013, 6(3): 549-563, https://doi.org / 10.5194/ amt-6-549-2013.

[24] CAO G Z, QI C L, MA G, et al. Mapping cloud mask of FY-3A VIRR to IRAS [J]. Remote Sensing Technology and Application, 2008, 23(1): 89-92 (in Chinese).

[25] LI J, ZOU X. A quality control procedure for FY-3AMWTS2 measurements with emphasis on cloud detection using VIRR cloud fraction [J]. J Atmos & Oceanic Technol, 2013, 30(8): 1704-1715 (in Chinese).

[26] YUAN Bing, FEI Jian-fang, WANG Yun-feng, et al. Experimental study on a dynamic asymmetrical typhoon initialization scheme based on 4D-Var [J]. J Trop Meteor, 2010, 16(4): 363-371, https://doi.org/10.3969/j.issn.1006-8775.2010.04.008.

Citation: YUAN Bing, MA Gang, ZHANG Peng, et al. A precipitation detection method for MWTS-II radiance assimilation in typhoon simulation [J]. J Trop Meteor, 2020, 26(2): 151-160, https://doi.org/10.46267/j.1006-8775.2020.014.